

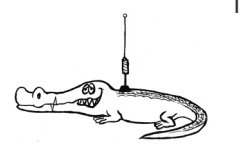
# Contents Guantum

	Editorial & Quotes	1
	Meet the School of Physics	1
<u>•</u>	From Napkins to Atomic Bombs Shaun Parasher	2
<b>(</b> -)	Selective Upregulation of HIF1-alpha Enhances Exercise Outcomes Diba Noorzad	3
0	Quantum Probability Measured Wayne Pooley	6
0	Quantum Double-Slit Experiment  Mani Shayestehfar	8
(c)	Puzzles Puzzlesoc	16
	Sponsors	17

Jeremy Team: Peter Lavilles, Mani Shayestehfar, Imasha Fernando, Stephanie Chen, Dorothy Serenity Nguyen, Lydia Zhang, Angela Liang, Aruna Sathyanarayanan Balaprabhavathi, and the PhySoc execs.



# JEREMY



Issue 2, 2025

The Physics Society Magazine

# **Editorial**

Jeremy Strikes Again! Or gets printed at a usual pace I guess... Or maybe your are reading this while you are taking a break at the Physics building's popular tea room just because your phone ran out of battery! Either way, our second issue of 2025 is all about the quantum world! We kick off with a quick peak into how Physicists use rough 'on the napkin' calculations to find surprisingly accurate estimates, for example, calculating the radius of an atomic blast. Also on an unprecedented turn, we get out of our comfort-zone, into biology, to read about the effect of a specific protein strand on diabetes by testing whether the protein enhances the exercise performance of mice. This is the first time we are including a non-physics/ mathematical article into Jeremy. We believe that this magazine should be an environment for ALL scientists to foster and share their work. We then teleport into the quantum realm with a mathematical dive into measure theory which clicks together the machinery behind quantum theory and oils up its wheels! We finally continue on the same note, by carefully investigating a famously misinterpreted gedankenexperiment (that's fancy German for 'thought experiment'), 'Wheeler's thought experiment', in quantum foundations. Let us know about your opinions and/or future ideas for Jeremy in the end. What did you like? What did you dislike? Or maybe both? Maybe the state of your satisfaction can be described as a superposition of linearly independent 'happy' and 'sad' states!

## Quote of the Issue

"mmm… smells like Crème Brûlée"

- Prof. Boris Kuhlmey

Cheeky context: Boris was demonstrating the effects of paramagnetism by torching a piece of metal (with something sweet on it, I guess?), and spoke the most French words known to man!

Would you like to publish your work? Whether it is a short and fun blurb, or a full-on scientific paper, *Jeremy* is a place to kick off your scientific ingenuity! Send your submissions to:

jeremy.physoc@gmail.com

# Meet the School of Physics



Meet Prof. Andrew Doherty! With a healthy obsession of the Roman Empire and a penchant for Italian food, Andrew has pioneered quantum control in the hope of there one day being a quantum computer. One of the best thing it will be able to do? Allow us to understand the chemistry of nitrogen-based fertilizer, and have a huge impact on resolving world hunger.



# From Napkins to Atomic Bombs

By Shaun Parasher

The phrase 'back of the napkin calculation' really gets a bad rep. It seems to imply that doing maths on a prosaic, hard-to-write-on object makes the calculation itself somehow disreputable or unstimulating. But, sometimes, taking weird hypotheticals and turning them into fun estimation problems can lead you in surprising directions in physics. This genre of problems is often called 'Fermi Problems', named after the illustrious Enrico Fermi and his uncanny ability to surmise the root of complex physics problems through a few, unreasonably precise assumptions and quick calculations.

In the early hours of July 16th of 1945, the crack team of physicists at Los Alamos were preparing to detonate the first ever atomic device in the white sands of the Alamogordo bombing range in New Mexico. Fermi, known for his subtly morbid sense of humour, ran a betting pool amongst the other physicists to see who could guess how many kilotons of TNT the euphemistically named 'gadget' yield would be equivalent to. The ascetic project director, J. Robert Oppenheimer, warily guessed 3 kilotons. The mercurial and irascible Edward Teller? A lofty 45.

The way Fermi tackled the problem was to drop a few pieces of paper at the moment the blast wave reached the observation site. With a rough guesstimate of the aerodynamics of paper, as well as the knowledge of the distance from the explosion, Fermi calculated the blast to be 10 kilotons, plus or minus 2.5. Not bad, considering the test released 20 kilotons. Unfortunately, Isidor Rabi took the pot with an unassuming punt of 18 kilotons. Achieving the same order of magnitude as the true bomb yield is hardly something to scoff at, though, considering the seemingly unorthodox method to arrive at it.



Ernest Lawrence, Enrico Fermi, and Isidor Rabi

A fun, adjacent Fermi Problem is to try to calculate the radius of an atomic bomb blast, without knowing the amount of energy released by fission products. For the bold, I would highly recommend trying it yourself. Making a few assumptions based on easy-to-work-with equations might see you waddling into success surprisingly quickly.

The British physicist, G.I. Taylor devised a method even simpler and less mathematically cumbersome than Fermi's paper snowflakes. Ignoring some of the effects of fission and adiabatic processes in the air that impede the blast wave, Taylor effectively reduced the problem into an applied physicist's playground. Being a wizened fluid dynamicist, he knew that the amount of released energy of the bomb would depend on the blast wave's velocity, the radius of the blast wave at a particular instant, and the density of the air. With some clever dimensional analysis, Taylor reduced the problem as such:

$$E = m \cdot \left(\frac{r}{t}\right)^2$$

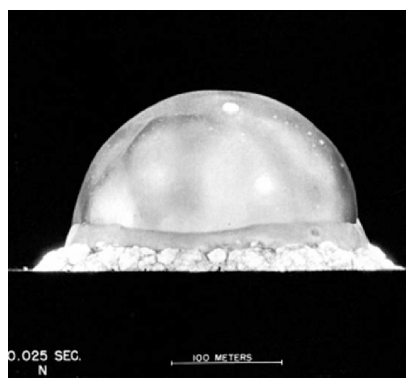
Where the energy E of the bomb that is dissipated by air is the mass multiplied by the velocity squared. We denote 'r' as the radius of the bomb, and 't' is just the time taken for the blast to travel some

distance.

$$ho = rac{m}{r^3}$$

The density  $\rho$  of air is equal to its mass divided by its volume.

Rearranging, we get  $E=
ho\cdot r^5/t^2$ . So,  $r=E^{\frac{1}{5}}\cdot t^{\frac{2}{5}}\cdot 
ho^{-\frac{1}{5}}$ .



The first ever Atom Bomb, 25 milliseconds after detonation

By measuring the radius of the bomb a few milliseconds after detonation, Taylor was able to calculate the time and length intervals of the bomb. Consequently, Taylor quite accurately guessed the yield of the atomic bomb to be 22 kilotons. One of the most closely guarded US military secrets was cracked by a British scientist using pen, paper and 4 lines of working out. Not bad for a back-of-the-napkin calculation.

Typically, all of Taylor's work was almost immediately seized, and he was strictly sworn to secrecy by the Military officials at Los Alamos. It was only in 1950 when he his papers detailing the 'Buckingham Pi' method of calculating the atomic bomb blast radius.

Sometimes, lots of unreasonably ambitious assumptions happen to cancel each other out, and enough dimensional analysis just might happen to accidentally reveal one of the most valuable pieces of information of World War Two.

### **References:**

- J. I. Katz, 'Special issue on the Manhattan Project Nuclear Science and Technology Development at Los Alamos National Laboratory', Nuclear Technology Volume 207, S326-S334 (2021).
- 2. Numberphile 2020, 'Bomb Blast Radius'
- Encyclopaedia Britannica, 'Sir Geoffrey Ingram Taylor'

### **Photo Credits:**

- 1. Fermi, Rabi, Lawrence, courtesy of the US Department of Energy
- 2. Atomic Bomb Detonation, courtesy of the US Department of Energy



# Selective Upregulation of HIF1-alpha Enhances Exercise Outcomes

By Diba Noorzad

### Introduction

Obesity is a growing global health concern. In Australia, 2014-15 data showed that 63.4% of adults and 27.6% of children were overweight or obese, with rates continuing to rise (Huse et al., 2018). Over the past 30 years, obesity rates have increased two- to threefold due to urbanization, sedentary lifestyles, and calorie-dense diets (Tiwari & Balasundaram, 2024).

Type 2 diabetes (T2D), primarily associated with obesity, arises from insufficient insulin production or insulin resistance, leading to high blood glucose. Sedentary lifestyles and high-fat diets have increased disease prevalence, straining both individuals and governments. In 2017-18, obesity cost Australia \$11.8 million, while T2D accounted for \$2.3 billion ("A framework for monitoring overweight and obesity in Australia, Summary," 2020).

Weight loss is the most effective intervention for T2D, with exercise playing a key role by improving insulin sensitivity, beta-cell function, and glycemic control (Holloszy, 2005; Kirwan et al., 2017). Exercise-induced oxygen depletion in skeletal muscles activates hypoxia-sensitive transcription factors, increasing hypoxia-inducible factor- $1\alpha$  (HIF- $1\alpha$ ) levels, which promote oxygen transport via erythropoietin and angiogenesis via vascular endothelial growth factor (Li, 2005; Ramakrishnan et al., 2014). HIF- $1\alpha$  has been linked to improved glucose-stimulated insulin secretion, yet diabetic tissues exhibit im-

paired HIF-1 $\alpha$  signaling (Catrina & Zheng, 2021). Given its role in exercise benefits and its dysfunction in diabetes, targeting HIF-1 $\alpha$  may improve metabolic outcomes.

HIF- $1\alpha$  is tightly regulated under nor moxic conditions via rapid degradation through the ubiquitin-proteasome system (Figure 1). Oxygen-dependent degradation is mediated by prolyl hydroxylase domain (PHD) proteins at proline residues (402 and 564) and by Factor Inhibiting HIF (FIH) at asparagine residue 803 (Gunton, 2020a; Huang et al., 1998). Hydroxylation marks HIF- $1\alpha$  for degradation via the von Hippel-Lindau (VHL) protein (Haase, 2009).

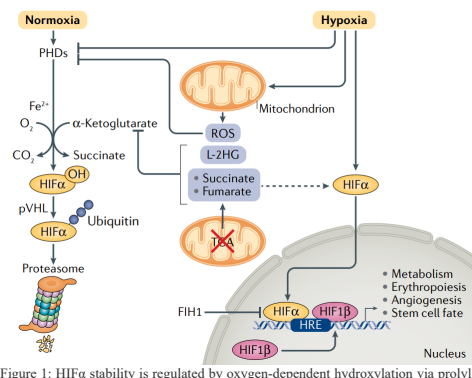


Figure 1: HIFα stability is regulated by oxygen-dependent hydroxylation via prolyl hydroxylases (PHDs), which mark it for degradation through the VHL complex under normoxia. In hypoxia, HIFα remains stable, pairs with HIF1β, and activates transcription of metabolic and survival genes. Mitochondrial ROS, L-2HG, and TCA cycle metabolites can further modulate HIFα stability by inhibiting PHD activity. Figure by (Lee et al., 2020).

HIF-1α upregulation can yield varying metabolic effects. VHL deletion impairs glucose metabolism, reducing insulin secretion and glucose uptake, leading to glucose intolerance (Cantley et al., 2009). Similarly, hepatocyte-specific VHL deletion causes exces-

sive vascular growth factor production, resulting in liver hemangiomas (Haase et al., 2001). PHD inhibition alters glucose metabolism by shifting β-cell energy production from glycolysis to fatty acid oxidation, disrupting insulin secretion under prolonged metabolic stress (Nasteska et al., 2021). In contrast, FIH deletion enhances oxidative metabolism, glycolysis, and insulin sensitivity, promoting improved metabolic responses (Sim et al., 2018). The authors demonstrated that FIH loss accelerates the hypoxic response by promoting metabolic shifts, initially increasing oxidative metabolism and glycolytic capacity but eventually suppressing oxidative metabolism under sustained hypoxia. Furthermore, FIH was found to act in concert with the PHD/VHL pathway to accelerate HIF-mediated responses, a mechanism particularly beneficial for tissues like skeletal muscle that experience high oxygen

Based on existing research, various methods of HIF-1α upregulation show different metabolic impacts depending on which residues are hydroxylated. When asparagine residues are hydroxylated, metabolic disruptions tend to occur, whereas hydroxylation at proline residues is often associated with more positive effects. This observation has led to our hypothesis that preventing asparagine hydroxylation could result in more favorable metabolic outcomes. A novel mouse model was created in the present study using CRIS-PR/Cas9 technology.

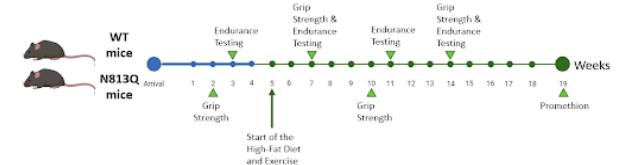


Figure 2: The experimental timeline

In this model, the asparagine residue at position 813 (equivalent to human Asp803) was mutated to glutamine, thereby preventing its hydroxylation. This study aims to compare the metabolic responses of N813Q mutant mice to wild-type (WT) controls to determine whether HIF-1 $\alpha$  enhances exercise performance.

### **Methods**

### Animal Husbandry

WT and N813Q mutant mice were acclimated for one week before baseline grip strength and endurance tests. At week 5, they were placed on a high-fat diet (45% lipid-based energy) and given running wheels for voluntary exercise. Grip strength and endurance tests were repeated at intervals (Figure 2). At week 19, metabolic and behavioral analyses were conducted using the Promethion system.

### Grip Strength

Grip Strength was measured using a grip strength meter, recording the highest value from three trials of five reps. Values were normalized to body weight.

### **Endurance**

Endurance Exercise Test was conducted on a 6-lane treadmill with an increasing speed protocol (starting at 3 m/min, increasing by 1 m/min per minute, maxing at 33 m/min at 10° incline). Testing ended when mice could no longer continue despite encouragement.

### Metabolic Analysis

Metabolic Analysis involved 48-hour monitoring in the Promethion system after 24-hour acclimation. Key outcomes included oxygen consumption (VO<sub>2</sub>), carbon dioxide output (VCO<sub>2</sub>), respiratory exchange ratio (RER), and energy expenditure (EE).

### Triglyceride Analysis

Triglyceride Analysis was performed using a colorimetric triglyceride assay kit (Abcam, USA) on plasma and quadriceps lysates. Samples were prepared, incubated with reagents, and measured at OD 570 nm.

### Histology

Quadriceps samples were fixed, paraffin-embedded, sectioned (5  $\mu$ m), and stained with hematoxylin and eosin. Images were analyzed using ImageJ for myofiber size and inter-myofiber spacing.

### Statistical Analysis

Data were analyzed using two-way ANOVA (genotype  $\times$  exercise) with Tukey's correction for multiple comparisons. Results are presented as mean  $\pm$  SEM, with significance set at p < 0.05.

### **Results**

### Grip Strength

No significant changes were observed in sedentary groups. While the WT-Ex group showed a slight increase, the mutant-exercise group exhibited a significant improvement over baseline (Figure 3).

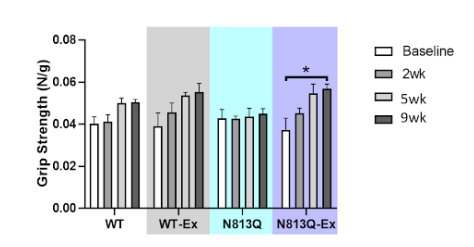


Figure 3: Grip strength measurements/improvement (normalized to mouse body weight) across different mouse cohorts. After 9 weeks of wheel running, N813Q-Ex mice had significantly improved grip strength compared to baseline values. Data were analyzed by mnANOVA with Tukey's post-hoc. \* p < 0.05 significant differences between two time points. Error bars represent the standard error of the mean (SEM). (This is true for all the graphs).

### Endurance

Sedentary groups showed no change. WT-Ex mice improved endurance over time, but N813Q-Ex mice displayed a more rapid increase, reaching WT-Ex levels in just two weeks (Figure 4).

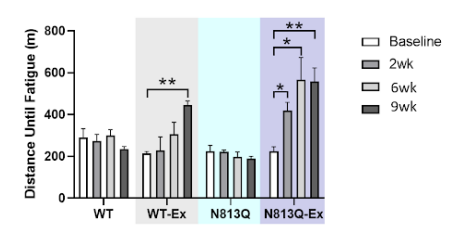


Figure 4: Endurance measurements across different mouse cohorts. After 9 weeks of wheel running, WT-Ex mice show a significant improvement in endurance. In comparison, the mutant mice also exhibit an increase in endurance, however, notably, the endurance outcome of 2 weeks of exercise in the mutants is similar to that of 9 weeks of exercise in the wild-type mice.

### Metabolic Analysis

No significant differences were found in EE, wheel distance, or speed, though exercise mice tended to run less 9 (Figure 5). N813Q-Ex mice showed a slight increase in EE.

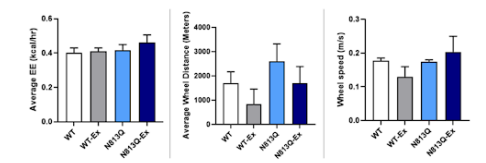


Figure 5: Energy expenditure, average wheel distance, and average wheel speed across four cohorts measured using the Promethion Metabolic Cage System. (A) Average energy expenditure (EE), (B) average wheel distance, and (C) average wheel speed. No significant changes were observed across any of the measurements.

### Triglycerides Qualification

Plasma triglyceride levels were similar across groups (Figure 6A). However, quadriceps triglycerides were significantly lower in all groups compared to WT-Sed (Figure 6B).

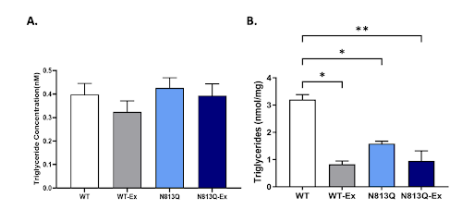


Figure 6: Triglyceride concentrations across the different groups. (A) Plasma triglyceride concentration (nM) and (B) quadriceps triglyceride concentration (nmol/mg) across different mouse groups. There is no significant difference in triglyceride plasma concentration among the groups. However, the triglyceride levels in the quadriceps of the sedentary wild-type group are significantly higher than those in the other three groups (WT-Ex, N813Q-Sed, and N813Q-Ex).

### Histology

Histological analysis was used to assess differences in myofiber size and inter-myofiber spacing across the groups. Representative hematoxylin and eosin staining images are shown in Figure 7A. No significant differences in myofiber size or inter-myofiber spacing were detected (Figures 7B & C). However, increased intra-myofiber lipid accumulation was observed in some groups.

### **Discussion**

Exercising muscle experiences significant hypoxia, emphasizing the critical role of HIF-1 $\alpha$  (Galkin et al., 2024). Knocking out HIF-1 $\alpha$  leads to impaired performance, muscle damage, and reduced metabolic activity (Mason et al., 2004), suggesting that increasing HIF-1 $\alpha$  by inhibiting its hydroxylation could enhance metabolism. While our findings partially support this, they also reveal complexities in HIF-1 $\alpha$  regulation.

N813Q mice exhibited greater grip strength than WT mice, indicating a metabolic ad-

vantage. However, this contradicts studies showing that HIF- $1\alpha$  upregulation via hypoxia reduces grip strength due to irisin downregulation and muscle atrophy (Kang et al., 2023; Liu et al., 2022). This discrepancy may be due to methodological differences, as hypoxia affects both asparagine and proline hydroxylation, whereas our study selectively inhibited asparagine hydroxylation.

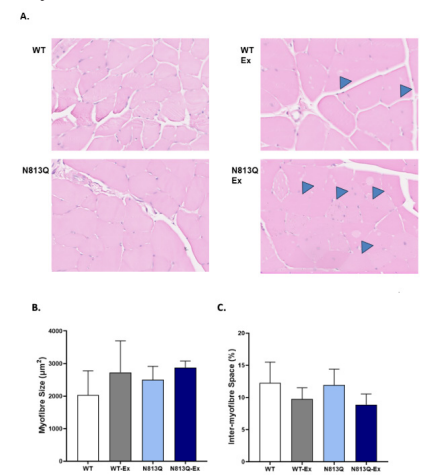


Figure 7: Quantification of quadriceps histology. (A) Representative section of quadriceps muscle across different mouse groups. Blue arrows indicate intramyofibrillar lipid deposits. The scale bar represents 100 μm. (B) Cross-section area of myofibers size (μm²) across different mouse groups. (C) Inter-myofiber space (%) across different mouse groups (i.e., the white space between the fibers). No significant differences in intermyofibrillar lipids were observed.

Interestingly, endurance significantly improved in N813Q mice, with their two-week running performance matching WT mice after nine weeks of training. This aligns with studies showing that long-term training increases FIH activity, reducing HIF-1 $\alpha$  via asparagine hydroxylation, which enhances aerobic metabolism (( Lindholm & Rundqvist, 2016; Mason & Johnson, 2007). Our results suggest that blocking asparagine hydroxylation may induce similar metabolic adaptations, improving endurance.

At week 19, non-exercised WT and N813Q mice showed greater voluntary running than their exercised counterparts, likely due to

novelty-driven activity. Despite shorter distances, N813Q-Ex mice exhibited higher speeds and slightly increased energy expenditure. This suggests a metabolic shift towards the Warburg effect, where HIF-1 $\alpha$  activation promotes glycolysis over oxidative phosphorylation, increasing glucose consumption and lactate production (Courtnay et al., 2015; Kierans & Taylor, 2021). Such metabolic reprogramming may enhance energy substrate availability and mitochondrial function, contributing to improved grip strength and endurance (Huang et al., 2022 , Semenza, 2011).

Despite a high-fat diet (HFD), plasma triglyceride levels remained unchanged across groups. However, sedentary WT mice had significantly higher quadriceps triglyceride concentrations, suggesting metabolic stability in the absence of exercise or HIF-1 $\alpha$  upregulation. Conversely, exercised groups, particularly N813Q mice, showed increased quadriceps lipid accumulation, consistent with the "elite athlete paradox," where enhanced lipid uptake supports fuel oxidation in insulin-sensitive individuals (Dubé et al., 2008; Gemmink et al., 2020, Li et al., 2019).

Histological analysis showed no significant myofiber size differences, though N813Q mice trended toward increased diameters. Similar findings in hypoxic catfish suggest HIF-1 $\alpha$  promotes muscle differentiation over proliferation (He et al., 2022; Xiao et al., 2023). However, species differences or experimental conditions may explain the lack of significant increases.

Additionally, a reduction in inter-myofiber space was observed in the exercised groups, particularly in the mutant exercised cohort, although this was not statistically significant. Reduced inter-myofiber space suggests increased muscle fiber packing density, pos-

sibly reflecting hypertrophy or enhanced muscle remodeling in response to exercise. This is consistent with findings by Sakushima et al. (2020) and Kumar et al. (2018) who reported that moderate hypoxia, which increases HIF-1 $\alpha$  expression, is associated with hypertrophy-related proteins and reduced inter-myofiber spacing (Kumar et al., 2018; Sakushima et al., 2020)

In conclusion, this study highlights the critical role of HIF-1α in mediating metabolic adaptations to exercise, particularly through the inhibition of asparagine hydroxylation. Our findings demonstrate that this targeted regulation enhances endurance capacity, potentially through the promotion of metabolic reprogramming and lipid utilization in skeletal muscle. These results suggest that fine-tuning HIF-1α activity could offer promising therapeutic strategies for improving exercise performance and managing metabolic disorders such as obesity and type 2 diabetes. However, the observed discrepancies with other models underscore the complexity of HIF-1a regulation, warranting further investigation to fully elucidate its context-dependent effects.

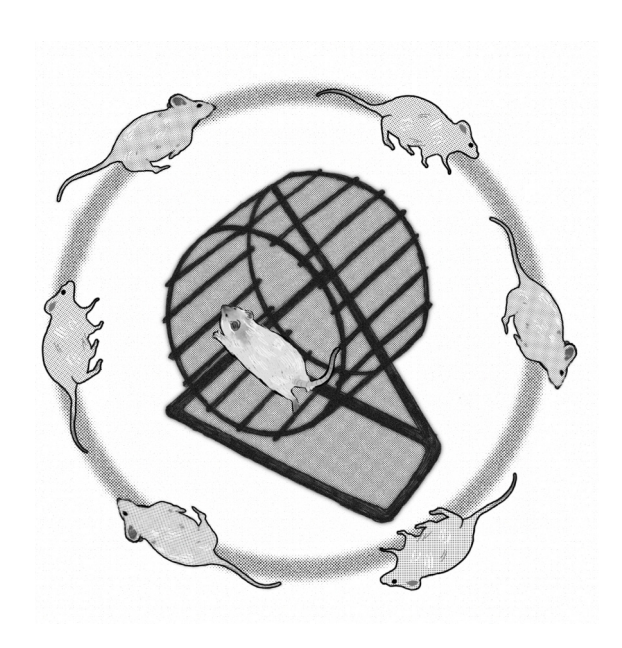
### Acknowledgements

I am deeply grateful to Dr. Josephine Yu and Prof. Jenny Gunton for their unwavering support, insightful feedback, and clear guidance throughout this Dalyell project. I also extend my sincere thanks to Dr. Yu and the team at the WIMR Centre for Diabetes, Obesity, and Endocrinology Research (CDOE) for their invaluable assistance in managing animal husbandry.

### References

Scan the OR code to see the references





### Quantum Probability Measured

Wayne Pooley

Exploring the pure mathematics background that underscores probability in quantum mechanics.

### I. INTRODUCTION

Quantum systems present themselves as some of the most mathematically interesting systems to be studied. Over the course of history, their mathematical descriptions have been fleshed out, allowing us to reap the benefits with simplified and elegant formalisms for calculating probabilities and expectation.

Measure theory is a field of mathematics that plays an important role in physics. It provides the language to rigorously define the physical ideas of mass, momentum, and probability in mathematical language. To illuminate intuition behind some of the familiar equations one comes across in undergraduate physics, we will explore measure theory's underpinning in quantum mechanics and look at a specific measure (the Projection-Valued Measure), all in a short-form style.

### II. MEASURE THEORY IN 5 MINUTES

In this section, we will see the motivation from measure theory that underlies the probability theory used. For physics students who have not done measure theory, I implore you to go through the properties of measures.

### Measure? $\sigma$ -algebra?

Measure theory is a branch of mathematics that generalizes notions of distance, length, area, and probability by abstracting integration. I will speed through some of the fundamentals of measure theory to provide some intuition and introduce the concepts that inform our descriptions of quantum systems.

Before we discuss what a "measure" is, let us discuss the domains on which they operate: " $\sigma$ -algebras". We let  $\mathcal{A}$  be a  $\sigma$ -algebra, defined over subsets of some set X. The  $\sigma$ -algebra consists of subsets of X, along with their respective set complements, the empty set, and must be closed under countable union.[1]

A measure is a set function  $\mu : \mathcal{A} \to \mathbb{K}$ , where  $\mathbb{K}$  is a codomain like the extended reals  $(\mathbb{R})$ . Briefly, measure  $\mu$  is monotonically increasing,  $\mu(\emptyset) = 0$ , and respects 'countable additivity'.[1]

Putting the previous concepts together, we define the measure space as  $(X, \mathcal{A}, \mu)$ . Different measure spaces utilize different measures and  $\sigma$ -algebras. Depending on our given system, we can change whether our measure maps to a subset of the extended real line, or some other codomain entirely. Using our measure spaces, we want to generalize integration, like making up for where the classical Riemann integral fails. 'Measurable functions' can be integrated to achieve this purpose. An application of this is in probability theory.

### **Probability Theory**

One important instance of a measure space is a 'probability space'. We can have a probability space  $(\Omega, \mathcal{A}, \mathbb{P})$ , where  $\Omega$  is our sample space and  $\mathcal{A}$  is a  $\sigma$ -field (same idea as  $\sigma$ -algebra) containing outcomes of events. The measure on this space  $\mathbb{P}: \mathcal{A} \to [0,1]$  is our probability measure. The probability space has the property  $\mathbb{P}(\Omega) = 1$ .

In the context of probability theory, measurable functions are called 'random variables'. These functions are important when defining measures with a density, where a measure  $\mu$  equals  $g(x)\nu$ - where g is a measurable function and  $\nu$  is a measure. [2]

Abstracting our integrals allows us to integrate functions over sets with respect to a measure. Thus, we can integrate with respect to our probability measure to find the expected value of a random variable:

$$\mathbb{E}[X] = \int_{\mathbb{R}} x \, d\mathbb{P}_X$$

using what we know about measures with a density, we can alter the above integral to take the form:

$$\mathbb{E}[X] = \int_{\mathbb{R}} x f(x) dx$$

where f is our probability density function and the integral in terms of the Lebesgue measure.[2]

We will find that the abstract integral form of the expected value is reflected when discussing our quantum systems using the projection-valued measure.

### III. PROJECTION-VALUED MEASURE

Okay, the meat and potatoes of the matter. Whatever you want to call it, this is the main conceptual chunk. Given some idea of what measure theory is and how it informs probability theory, let us look at the axioms for the projection-valued measure, then see how we derive expressions for expectation and probability in quantum mechanics.

### Definition 1

The projection-valued measure (PVM) [3] on  $\mathbb{R}$  is a map  $P: \mathcal{B}(\mathbb{R}) \to \mathcal{L}(\mathcal{H})$  from the Borel  $\sigma$ -algebra,  $\mathcal{B}(\mathbb{R})$ , to the space of bounded linear operators on the Hilbert space  $\mathcal{H}$  with properties:

1.  $\forall B \in \mathcal{B}(\mathbb{R}), P(B)$  is an orthogonal projection:  $P(B) = P(B)^2$  and self-adjoint  $P(B) = P(B)^*$ .

2.  $P(\emptyset) = 0$ ,  $P(\mathbb{R}) = I$ , where I is the identity operator.

3. For  $B_i, B_j \in \mathcal{B}(\mathbb{R})$  where  $B_i \cap B_j = \emptyset$  for  $i \neq j$ ,

$$P\left(\bigcup_{n\in\mathbb{N}}B_n\right) = \sum_{n=1}^{\infty}P(B_n)$$

Similar to the previous concept of a real-valued measure that returns scalars in  $\mathbb{R}$ , the PVM measures sets in the space and returns self-adjoint projections associated with that observable's operator, say  $\hat{A}$  in this case.[4] Specifically, if the Borel  $\sigma$ -algebra corresponds to measurable outcomes for a given observable, then for some Borel set  $B \in \mathcal{B}(\mathbb{R})$ , P(B) corresponds to an operator whose eigenvalues are a subset of the measurable outcomes of the original observable  $\hat{A}$ . This means that P maps  $|\psi\rangle$  to subspaces of  $\mathcal{H}$ .[4]

For example, take a simple discrete binary system: spin up and down. The eigenvalues for the spin operator associated with this observable are  $\{\pm 1\}$ . We can get the operators

$$P(\{+1\}) = |+\rangle \langle +|$$

$$P(\{-1\}) = |-\rangle \langle -|$$

where  $|-\rangle$  and  $|+\rangle$  span the state space.

Therefore, if we take some arbitrary state vector  $|\psi\rangle$ , then the projection-valued measure acting on this vector maps it to a subspace of the Hilbert space:

$$P(\{+1\}) |\psi\rangle = (|+\rangle \langle +|)(\alpha |+\rangle + \beta |-\rangle)$$
$$= \alpha |+\rangle$$

where  $\alpha, \beta \in \mathbb{C}$ . (Note this new state isn't inherently normalized). Similar argument for  $P(\{-1\})$ .

### PVM's in Probability

We also get the form for the probability for observing a given outcome  $B \in \mathbb{R}$  (a range of eigenvalues):

Probability(B) = 
$$||P(B)|\psi\rangle||^2$$
  
=  $\langle \psi | P(B)^2 | \psi \rangle$   
=  $\langle \psi | P(B) | \psi \rangle$   
=  $\langle \varphi | \psi \rangle$ .

 $|\varphi\rangle$  is the projection of  $|\psi\rangle$  to a subspace of  $\mathcal{H}$ .

Expectation value is defined as the weighted sum:

$$\mathbb{E}(\hat{A}) = \sum_{n=0}^{\infty} \lambda_n \langle \psi | P_n | \psi \rangle$$
$$= \langle \psi | (\sum_{n=0}^{\infty} \lambda_n P_n) | \psi \rangle$$
$$= \langle \psi | \hat{A} | \psi \rangle$$

The above derivation utilizes the spectral theorem in the third line. We can generalize the above result to a continuous spec-

r. trum:

$$\begin{split} \left\langle \psi \right| \hat{A} \left| \psi \right\rangle &= \int_{\mathbb{R}} \lambda \left\langle \psi \right| dP(\lambda) \left| \psi \right\rangle \\ &= \int_{\mathbb{R}} \lambda d(\left\langle \psi \right| P(\lambda) \left| \psi \right\rangle) \end{split}$$

Here is the key, we can treat  $\langle \psi | P(\lambda) | \psi \rangle$  as a probability measure as it adheres to the rules of a probability measure.[5] This allows us to show equivalence between the expectation value above and the expected value from the probability theory section, as they both relate to integrating a variable with respect to a probability measure.[6]

Here is quick reminder of the Spectral Theorem from the previous derivation. It states that any Hermitian operator  $\hat{H}$  can be expressed as

$$\hat{H} = \int_{\operatorname{spec}(\hat{H})} \lambda dP(\lambda)$$

where  $\lambda$  are the observable's eigenvalues (a generalization of the set of eigenvalues), spec( $\hat{H}$ ) is the spectrum of  $\hat{H}$ , and  $dP(\lambda)$  is the projection-valued measure of the observable.[6]

### BUT WAIT, THERE'S MORE!

PVM's have plenty of applications in proofs in quantum mechanics beyond what I have covered in this article. We have seen this measure used in simple concepts of probability, but it has tie-ins into advanced topics like systems of quantum-identical particles.

PVMs have a further generalization that being Positive Operator-Valued Measures (POVMs). POVMs are measures whose values are positive semi-definite operators on a Hilbert space. They can be used in advanced proofs in quantum field theory or quantum information theory. They also have applications in simpler systems. For instance, if you wanted to reconstruct an unknown state by performing measurements, a process known as state tomography, you can employ POVMs to improve efficiency.[7]

The story of how measures inform quantum theory is a deep and rich area of mathematics and physics. I hope to have helped bring forth some of the interesting ideas for your consideration and as a nice form of small talk next time you're at the water cooler.

### IV. ACKNOWLEDGEMENTS

I would like to thank my supervisor, Dr. Abhijeet Alase, for their invaluable help in proofreading this work and for introducing key concepts that shaped its direction. I am also grateful to Nelson Odins-Jones for providing essential resources that enriched the content. Lastly, I extend my appreciation to everyone who has taken the time to review and provide feedback on various versions of this work—your insights have been greatly appreciated.

<sup>[1]</sup> S. Mehling, An introduction to measure theory and its applications in physics (2018), university of Chicago REU Paper.

<sup>[2]</sup> D. Daners, Measure Theory and Fourier Analysis (School of Mathematics and Statistics, The University of Sydney, 2023).

<sup>[3]</sup> L. A. Takhtajan, Lecture notes on mathematical methods of classical mechanics, in MAT 570, Spring 2006 (2006).

 <sup>[4]</sup> B. C. Hall, Quantum Theory for Mathematicians, Graduate Texts in Mathematics, Vol. 267 (Springer, 2013).

<sup>[5]</sup> L. A. Takhtajan, Quantum Mechanics for Mathematicians, Graduate Studies in Mathematics, Vol. 95 (American Mathematical Society, 2008).

<sup>[6]</sup> W. Rudin, Functional Analysis, 2nd ed. (McGraw-Hill, 1991).

<sup>[7]</sup> M. A. Nielsen and I. L. Chuang, Quantum Computation and Quantum Information, 2nd ed. (Cambridge University Press, Cambridge, 2010).

### The Double-Slit Delayed-Choice Experiment: A Classical Innovation

Mani Shayestehfar, Sasha Kurakin

The foundations and thus the strangest notions in quantum physics lie within the model's divergences from the classical theory of light. Where certain experiments may appear to be inherently quantum mechanical in nature, beyond the surface level they can be explained using purely classical theory. We explore the "Double-Slit Experiment" with an adaptation from Wheeler's "Delayed-Choice Experiment". We remodel and propose an analogue experiment that retrieves the time-measured double-slit results, including interference patterns and which-path information using Jones calculus and its classical analysis.

### Background

### -Motivation -

Quantum mechanics rises in areas where a classical theory of light cannot comprehensively describe the relevant phenomena. In the "classical" theory, light can be described as the propagation of linearly independent electric and magnetic wave components in space and time. Where the classical interpretation diverges, the quantum theory provides a satisfactory explanation for various phenomena that otherwise could not be explained. The dependence of measurement outcomes on the observer's role in quantum mechanics, shows fundamental discrepancies between the classical and quantum theories, that require further investigation. As such, many quantum interpretations appear to be different to that of the classical theory. We attempt to answer the following questions: Is it possible to decompose non-classical predictions to their core to unveil a simpler explanation compared to what quantum mechanics offers? Which physical phenomena can be investigated? Will the predictions agree in their relative causal structures?

In this paper, we consider the "Delayed-Choice Double-Slit experiment" by proposing an analogous experiment that adapts the former investigation by Pantaleoni (2016) [7], while only relying on purely classical theory. We compare our findings, highlighting areas where similar results are retrieved, areas where differences lie, and the structural differences between the two approaches.

### - The Double-Slit Experiment -

First investigated by Thomas Young, the "Double-Slit Experiment" (DSE) is a notable demonstration of the wave-particle duality of light. Although many variations of the experiment exist, the double-slit experiment involves a coherent, monochromatic light source incident on a barrier with two sufficiently narrow slits, as well as a screen positioned behind the barrier which records the incident pattern of light on it (FIG.1). The experiment follows the Fraunhofer regime  $(L \gg \delta)$ , where  $\delta$  is the slit width and L is the distance between the barrier and the screen. [2] For a Gaussian laser light source with a

short pulse, the experiment can be investigated using the two models. Light can classically be modelled as an electromagnetic wave propagating towards the barrier. For a fixed direction r, this is denoted as  $E(t) = E_0 e^{i(k_0 r - \omega t + \phi)}$  where  $k_0 = \frac{2\pi}{\lambda}$  and  $\phi$  are respectively the free-space wavevector, and phase term. Given a wave function E(t), the intensity at a point is a function of a phase difference  $\epsilon$  between the waves from each slit. Hence the intensity is

$$I = ||E(t) + E(t)e^{i\epsilon}||^2 \tag{1}$$

$$= (E(t) + E(t)e^{i\epsilon})(E^*(t) + E^*(t)e^{-i\epsilon})$$
 (2)

$$=E_0^2(2+2\cos\epsilon)\tag{3}$$

After diffracting through the slits, the two new propagating wavefronts interfere constructive/destructively to form bright/dark fringes on the screen. The path difference between the waves,  $\Delta s = m\lambda$  where  $\lambda$  denotes the light wavelength is equivalent to the phase difference of light due to a delayed time of arrival to a point on the screen, which causes the resultant double-slit pattern. For m = 1, 2, 3, ... this yields:

$$\Delta s = \begin{cases} m\lambda & \text{constructive} \\ (m - \frac{1}{2})\lambda & \text{deconstructive} \end{cases}$$

Given a single photon source, the wave-like behaviour of photons is unexpected. Considering a quantum analysis, before placing a detector in front of a slit, the photon is in a superposition at the two slit locations  $x_1$  and  $x_2$ .

$$|\psi\rangle = \frac{1}{\sqrt{2}} (|x_1\rangle + |x_2\rangle)$$
 (4)

Delocalisation in the momentum distribution of light projected onto the detection screen, results in an interference pattern.

$$\langle \hat{p}|\psi\rangle = \frac{1}{\sqrt{2}} \left(\langle \hat{p}|x_1\rangle + \langle \hat{p}|x_2\rangle\right)$$
 (5)

$$= \frac{1}{\sqrt{2}} \left( F_{\delta}(x_1) + F_{\delta}(x_2) \right) \tag{6}$$

where  $\hat{p}$  is the momentum operator,  $\delta$  is the finite width of each slit, and  $F(x_i)$  is the Fourier transform at slit i onto the momentum space [4]. If a measurement is made on a position basis, information about this distribution

will disappear, as by Heisenberg's uncertainty principle, position and momentum are not commuting, and the particle pattern is retrieved. The **which-path information** (**WPI**) is the information available regarding the path that light takes through either slit. WPI is correlated to the availability of the interference pattern. In FIG.1(a), the traveled paths are indistinguishable and interference information is available. In FIG.1(b) the contrary is true and WPI is available and distinguishable [8]. The combination of classical and quantum models provides a sufficient but disjoint interpretation of the experiment.

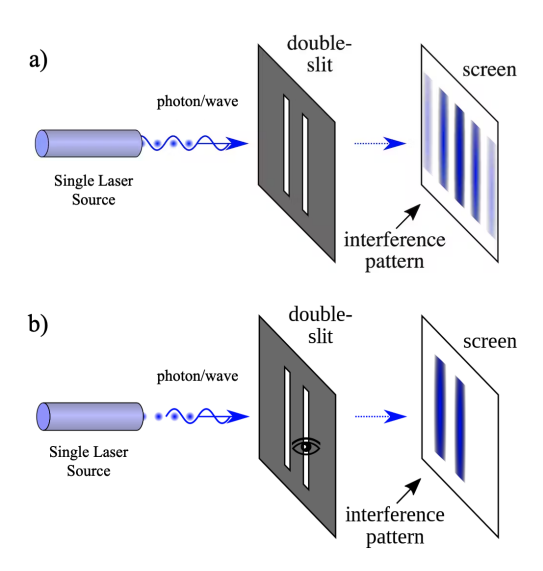


**FIG. 1:** Simplified schema of the DSE with **a)** no detector in place (WPI available) and **b)** detector in front of a slit (WPI unavailable) (*Image source: Johannes Kalliauer (2017)*)

### - Wheeler's Delayed-Choice -

In the 1980s John Archibald Wheeler proposed a Gedanken experiment to investigate the causal significance of the observer in the measurement collapse [9]. In a variation of the proposal, coherent and monochromatic light is incident on a Mach–Zehnder interferometer setup. The incident mode is split into reflected and transmitted components via the first beam-splitter which travel paths with equal length. The observer is then granted a "choice" to place a second beam-splitter or not before the two light detectors (FIG.2). The experiment is analogous to the DSE in nature and demonstrates the wave-particle duality of light depending on the presence of the second beam-splitter.

In the case where the second beam-splitter is not present, each detector registers events 50% of the time, with no simultaneous detections occurring. Wheeler interprets this as the light "photon" either probabilistically reflecting or transmitting at the first beam-splitter, then travelling through one of the arms and thus yielding the detection result. Hence, the placement choice results in a particle behaviour. In the case where the beam-splitter is present, detection at only one detector is observed.

This is interpreted as EM waves splitting to transmission and reflection modes upon arriving at the first beam splitter. Reflection modes change in phase and thus two arms host light of differing phases. After arriving at the second beam-splitter, deconstructive interference of light results in no detection at one detector, while constructive interference results in detection. Note that the type of detection here is not strictly defined and is subject to the experiment. Wheeler interprets this as a wave behaviour of light.

The "delayed choice" for the presence of the removable beam-splitter poses a potential causal problem. Given the lack of the beam-splitter, one may assume that light will behave as a particle. However, if the observer inserts the beam-splitter after the light has entered the system, a wave detection pattern is observed. One can evaluate this result to be retrocausal as the entered photon would require to move back in time to change its subsequent behaviour [1]. But can the observations be explained without any reliance on retrocausal structures?

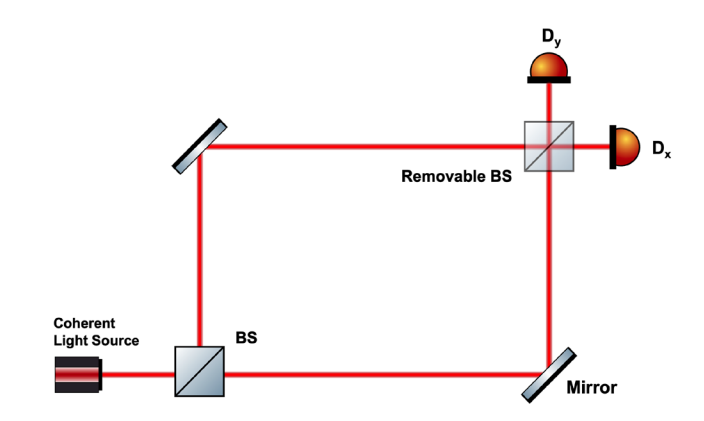


FIG. 2: A variation of Wheeler's thought experiment with the top-right beam-splitter determining the delayed-choice behaviour of light.

### Approach

### $-\ The\ Proposed\ Jones\ Calculus\ -$

For the light propagating through the system, we consider a Jones Vector representation for the polarisation state of light. The orthogonal polarisation directions are defined with the basis  $\mathcal{P} = \{|H\rangle, |V\rangle\}$  [Note1] where  $|H\rangle$  and  $|V\rangle$  represent orthogonal horizontal and vertical directions of polarisation respectively. The Cartesian direction of light propagation in horizontal/vertical arms (orthogonal x, y directions) regardless of the sign is defined by the basis  $\mathcal{D} = \{|X\rangle, |Y\rangle\}$ . The tensor product on the space of polarisation and propagation yields a basis for the elements of  $\mathcal{B}$  in  $\mathbb{C}^4$  as such:

$$\mathcal{P} \otimes \mathcal{D} = \mathcal{B} = \{ |H\rangle |X\rangle, |H\rangle |Y\rangle, |V\rangle |X\rangle, |V\rangle |Y\rangle \} \quad (7)$$

where

$$\begin{aligned} |H\rangle |X\rangle &= & \begin{bmatrix} 1 & 0 & 0 & 0 \end{bmatrix}^T \\ |H\rangle |Y\rangle &= & \begin{bmatrix} 0 & 1 & 0 & 0 \end{bmatrix}^T \\ |V\rangle |X\rangle &= & \begin{bmatrix} 0 & 0 & 1 & 0 \end{bmatrix}^T \\ |V\rangle |Y\rangle &= & \begin{bmatrix} 0 & 0 & 0 & 1 \end{bmatrix}^T \end{aligned}$$

The purpose behind this basis definition is to define each optical element's operation (Appendix ) on light using matrices  $Mat_{4\times4}(\mathbb{C})$  acting on a Jones Vector representation of input light (FIG.3).

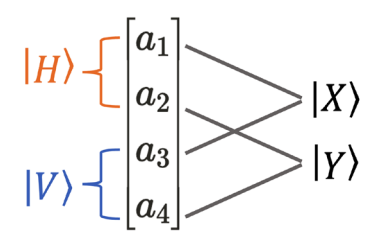


**FIG. 3:** Coordinates representation in the defined basis  $\mathcal{B}$  of polarisation and propagation direction. For  $i \in [1, 4], \ a_i \in \mathbb{C}$ .

### - The Proposed Analogue -

To construct a delayed-choice analogue experiment, we are motivated by a setup from Pantaleoni G. (2017). As shown in FIG.4, a Gaussian beam is emitted from the laser source, propagating through the system at two different paths incident on a diagonal polariser at 45°. The light is then incident on a beam-splitter (BS) which splits light into distinctive short and long paths (straight down, and reflected from mirrors). After arriving at a polarised beam-splitter (PBS1), some light components reach a Quarter Waveplate (oriented at  $\theta^{\circ}$ ), Send-Back Mirror, Quarter Waveplate setup (QWP-SBM-QWP) and are then reflected back to PBS1. Components then travel once more to BS, where some components arrive at a Variable Waveplate (VWP) imparting a variable phase  $\varepsilon$  only to the  $|V\rangle$  component. The light is then incident on a Half Waveplate (HWP) oriented at 22.5° which constructs diagonal/anti-diagonal light. Upon a phase shift, light is finally incident on another polarised beam-splitter PBS2 which leads to detection at two orthogonal detectors.

### - Pre-QWP -

The light becomes diagonally-polarised  $((|H\rangle + |V\rangle)|Y\rangle \rightarrow |+\rangle|Y\rangle)$  after the polariser. The proposed light source emits a Gaussian envelope with the function  $f(t,\sigma,l)=\exp(-\frac{(ct-l)^2}{2\sigma^2})$  where c and  $\sigma$  are the speed and standard deviation of light respectively and l is the distance from the polariser, resulting in the interferometer's input light as

$$E(t) = f(t, \sigma) |+\rangle |Y\rangle.$$
 (8)

The beams-plitter BS equally splits incident intensties, applying  $\frac{\pi}{2}$  phase shift in the reflected mode (Appendix 1). The overall (time-independent) polarisation state is then

$$\vec{\psi} = \frac{1}{\sqrt{2}} \ket{+} (\ket{X} + i \ket{Y}) \tag{9}$$

Given there is path length difference between the short and long arm (FIG.4), the component  $\frac{1}{\sqrt{2}}|+\rangle|X\rangle$  will arrive at PBS1 with a time delay  $\tau=2d/c$  where d is the distance from BS to the first mirror. By definition, the polarising beam-splitter PBS1 only reflects  $|V\rangle$  (with another phase gain) and transmits  $|H\rangle$ . This results in a loss of half of the intensity that arrives from each arm, as short (long) propagation leads to a loss of vertical (horizontal) component which exits the system. Hence after PBS1

$$\frac{1}{\sqrt{2}} \ket{+} \ket{Y} \to \frac{1}{2} \ket{H} \ket{Y} \tag{10}$$

$$\frac{i}{\sqrt{2}} \ket{+} \ket{X} \to -\frac{1}{2} \ket{V} \ket{Y}$$
 (after time  $\tau$ ) (11)

$$\therefore \vec{\psi} = \frac{1}{2} (|H\rangle - |V\rangle) |Y\rangle \tag{12}$$

### -QWP-SBM-QWP -

The Quarter Waveplate, Send-Back Mirror, Quarter Waveplate setup is a field standard for polarisation state switching. The presence (absence) of the QWP is analogous to Wheeler's presence (absence) of the removable beam-splitter. When oriented at an angle  $\theta$  about the horizontal polarisation axis, the light undergoes a  $\frac{\pi}{2}$  phase shift. The SBM then reflects the light and introduces another phase gain of  $\pi$  on the vertical component. After reflection, the light is again incident on the QWP at an angle  $\pi - \theta$  (due to reflection). This acts to swap the singular  $|H\rangle$  and  $|V\rangle$ 's arm paths with Short  $(|H\rangle) \leftrightarrow Long$   $(|V\rangle)$ . This yields

Short 
$$|H\rangle \longrightarrow -\sin(2\theta)|V\rangle$$
 (13)

$$Long |V\rangle \longrightarrow \sin(2\theta) |H\rangle$$
 (14)

after re-entering PBS1 and respectively reflecting/transmitting. Ignoring the intensity loss, this implies that the polarisation state at each traversed arm is now reversed, and hence the components will arrive back at BS at the same time as the time delay  $\tau$  is reversed. The light taking the *Short-Long* and *Long-Short* no longer contains distinguishable WPI due to the superposition of the two paths which is analogous to the presence of the double-slit pattern in the DSE. Substantially, the rotation of QWP along its optical axis is equivalent to adjusting the intensity of light at a point on the DSE screen, with max/min intensities corresponding with the presence of WPI.

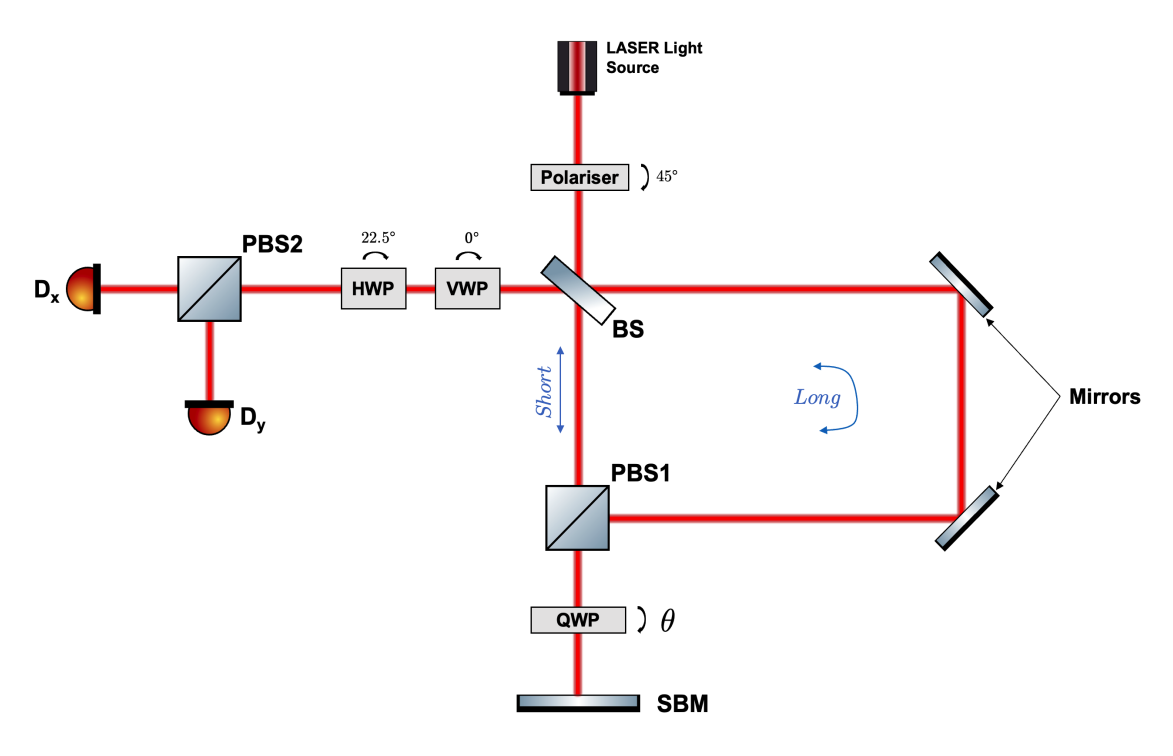


**FIG. 4:** The overall schema of the analogue setup. The straight lines represent the propagation of light through the interferometer arms. Angles shown for Polariser, QWP and HWP are with respect to the horizontal polarisation axis. The detectors on the left are orthogonal and identical in path length to PBS2. The *Short* and *Long* paths are demonstrated.

It is known that for specific  $\theta$  values, the path distinguishability is maximised. Notably, this occurs when the  $|H\rangle$  and  $|V\rangle$  components respectively take Short-Short and Long-Long paths as the Long-Long path will arrive with a time delay of  $2\tau^{[\text{Note2}]}$ . In this configuration the presence of time-dependent WPI is analogous to applying a measurement on one of the slits in the DSE, and hence losing the momentum space projection on the screen. The polarisation states of light until after the second passage through PBS1 ( $|V\rangle$  component phase gain) in time-order are:

$$\vec{\psi}_{Short\text{-}Short} = \frac{1}{2} |H\rangle |Y\rangle \longrightarrow \frac{\cos 2\theta}{2} |H\rangle |Y\rangle$$
 (15)

$$\vec{\psi}_{Short\text{-}Long} = \frac{1}{2} |H\rangle |Y\rangle \longrightarrow -\frac{i\sin 2\theta}{2} |V\rangle |X\rangle$$
 (16)

$$\vec{\psi}_{Long\text{-}Short} = -\frac{1}{2} |V\rangle |Y\rangle \longrightarrow -\frac{\sin 2\theta}{2} |H\rangle |Y\rangle$$
 (17)

$$\vec{\psi}_{Long\text{-}Long} = -\frac{1}{2} |V\rangle |Y\rangle \longrightarrow -\frac{i\cos 2\theta}{2} |V\rangle |X\rangle$$
 (18)

One can importantly notice that for  $\theta=(2k-1)\frac{\pi}{4}$  where k is an integer, the *Short-Short* and *Long-Long* polarisation states vanish, while for  $\theta=k\frac{\pi}{2}$ , the *Short-Long* and *Long-Short* states vanish. Thus the rotation of QWP ultimately determines the state of which-path information and hence the interference pattern.

### - Interference Detection -

Upon 'polaristation swapping', PBS1 splits each orthogonal component by transmitting  $\vec{\psi}_{Long-Short}$  and reflecting  $\vec{\psi}_{Short-Long}$  with another  $\frac{\pi}{2}$  phase gain as shown in eq. (13) & (15).

With the time-delay between  $\vec{\psi}_{Long\text{-}Short}$  and  $\vec{\psi}_{Short\text{-}Long}$  now resolved, the states are incident at BS simultaneously while  $\vec{\psi}_{Short\text{-}Short}$  and  $\vec{\psi}_{Long\text{-}Long}$  states are distinguishable in time as discussed before. At BS, intensity loss in two components of light (i.e.  $|V\rangle$  from  $\vec{\psi}_{Short\text{-}Long}$  and  $|H\rangle$  from  $\vec{\psi}_{Long\text{-}Short}$ ) equates to  $\frac{1}{\sqrt{2}} \cdot \frac{1}{\sqrt{2}} = \frac{1}{2}$ . This leads to an overall (and final) intensity efficiency of  $\frac{1}{2} \cdot \frac{1}{2} = \frac{1}{4}$  for the system. The polarisation states in time-order after BS are:

$$\vec{\psi}_{Short-Short} = \frac{i\cos 2\theta}{2\sqrt{2}} |H\rangle |X\rangle \tag{19}$$

$$\vec{\psi}_{Short\text{-}Long} = -\frac{i\sin 2\theta}{2\sqrt{2}} |V\rangle |X\rangle \tag{20}$$

$$\vec{\psi}_{Long\text{-}Short} = -\frac{i\sin 2\theta}{2\sqrt{2}} |H\rangle |X\rangle$$
 (21)

$$\vec{\psi}_{Long\text{-}Long} = -\frac{i\cos 2\theta}{2\sqrt{2}} |V\rangle |X\rangle \tag{22}$$

where we notice that  $\vec{\psi}_{Short-Long} = \vec{\psi}_{Long-Short}$  as expected.

Arriving at the VWP which is set parallel to the

horizontal polarisation axis, the polarisation states undergo a variable phase gain  $\varepsilon$  to their  $|V\rangle$  such that  $|V\rangle|X\rangle \longrightarrow e^{i\varepsilon}|V\rangle|X\rangle$  (See Appendix 1 ). The polarisation states in time-order are now:

$$\vec{\psi}_{Short-Short} = \frac{i\cos 2\theta}{2\sqrt{2}} |H\rangle |X\rangle \tag{23}$$

$$\vec{\psi}_{Short\text{-}Long} = -\frac{i\sin 2\theta}{2\sqrt{2}} e^{i\varepsilon} |V\rangle |X\rangle \tag{24}$$

$$\vec{\psi}_{Long\text{-}Short} = -\frac{i\sin 2\theta}{2\sqrt{2}} |H\rangle |X\rangle \tag{25}$$

$$\vec{\psi}_{Long\text{-}Long} = -\frac{i\cos 2\theta}{2\sqrt{2}} e^{i\varepsilon} |V\rangle |X\rangle$$
 (26)

The HWP oriented at  $\frac{\pi}{8}$  causes incident  $|H\rangle|X\rangle \rightarrow |+\rangle|X\rangle$ , and  $|V\rangle|X\rangle \rightarrow |-\rangle|X\rangle$  where  $|-\rangle$  is anti-diagonal polarisation. Finally, PBS2 operates similar to PBS1 to separate orthogonal polarisation components where all  $|H\rangle$  and  $|V\rangle$  components are detected by  $D_x$  and  $D_y$  respectively. Of course, the reflection phase gain must again be considered.

The final polarisation states can be evaluated on a detector basis in time-order. At  $D_x$ :

$$\vec{\psi}_{Short-Short} = \frac{i\cos 2\theta}{4} |H\rangle |X\rangle \tag{27}$$

$$\vec{\psi}_{Short\text{-}Long} = -\frac{ie^{i\varepsilon}\sin 2\theta}{4} |H\rangle |X\rangle$$
 (28)

$$\vec{\psi}_{Long\text{-}Short} = -\frac{i\sin 2\theta}{4} |H\rangle |X\rangle \tag{29}$$

$$\vec{\psi}_{Long\text{-}Long} = -\frac{ie^{i\varepsilon}\cos 2\theta}{4} |H\rangle |X\rangle \tag{30}$$

And at  $D_y$ :

$$\vec{\psi}_{Short\text{-}Short} = \frac{\cos 2\theta}{4} |V\rangle |Y\rangle \tag{31}$$

$$\vec{\psi}_{Short-Long} = -\frac{e^{i\varepsilon}\sin 2\theta}{4} |V\rangle |Y\rangle \tag{32}$$

$$\vec{\psi}_{Long\text{-}Short} = \frac{\sin 2\theta}{4} |V\rangle |Y\rangle \tag{33}$$

$$\vec{\psi}_{Long\text{-}Long} = -\frac{e^{i\varepsilon}\cos 2\theta}{4} |V\rangle |Y\rangle \tag{34}$$

### Discussion

### - $\boldsymbol{Analysis}$ -

The correspondence between the proposed analogue and the classical model lies within achieving similar interference and WPI results while maintaining a cohesive causal structure. Recall that the *Short-Long* and *Long-Short* configurations have a similar total distance and so

the polarisation states through each configuration will arrive in phase at the detectors. The total wave intensities at time t given by  $I_x(t)$  and  $I_y(t)$  at each detector can be described as the multiplication of the Gaussian function and the evolved polarisation states for all configurations.

$$I_{x} = \|f(t,\sigma,l)\vec{\psi}_{Short-Short} + f(t,\sigma,l+2d)(\vec{\psi}_{Short-Long} + \vec{\psi}_{Long-Short}) + f(t,\sigma,l+4d)\vec{\psi}_{Long-Long}\|^{2}$$

$$= \|f(t,\sigma,l)\frac{i\cos 2\theta}{4}$$

$$- f(t,\sigma,l+2d)\frac{i\sin 2\theta}{4}(1+e^{i\varepsilon})$$

$$- f(t,\sigma,l+4d)\frac{\cos 2\theta}{4}ie^{i\varepsilon}\|^{2}$$

$$I_{y} = \|f(t,\sigma,l)\vec{\psi}_{Short-Short} + f(t,\sigma,l+2d)(\vec{\psi}_{Short-Long} + \vec{\psi}_{Long-Short}) + f(t,\sigma,l+4d)\vec{\psi}_{Long-Long}\|^{2}$$

$$= \|-f(t,\sigma,l)\frac{\cos 2\theta}{4} + f(t,\sigma,l+2d)\frac{\sin 2\theta}{4}(1-e^{i\varepsilon})$$

$$- f(t,\sigma,l+4d)\frac{\cos 2\theta}{4}e^{i\varepsilon}\|^{2}$$

where the variables are defined as before and the polarisation states are used from the final detector outputs. Importantly, the intensity equations determine that  $\theta$  impacts the intensity of each polarisation state  $\vec{\psi}$  and  $\varepsilon$  from the VWP impacts the phase difference for each path.

### $-DSE\ Comparison-$

Upon understanding the role of  $\varepsilon$  and  $\theta$  we may derive similarities between the DSE and the analogue. The role of  $\varepsilon$ , as discussed, is to input a relative phase between the polarisation and hence between the different paths.  $\Delta \varepsilon$  can then be used to change the interference pattern through its peak intensity (Fig.5). Recall that for the no WPI case, the total detection (i.e  $\vec{\psi}_{Short-Long} + \vec{\psi}_{Long-Short}$ ) of the polarisation states at the detectors are:

$$D_x : -\frac{i\sin 2\theta}{4} (1 + e^{i\varepsilon}) |H\rangle |X\rangle$$

$$\implies I_{peak,x} = \frac{\sin^2 2\theta}{8} (1 + \cos \varepsilon)$$

$$D_x : \frac{\sin 2\theta}{4} (1 - e^{i\varepsilon}) |V\rangle |Y\rangle$$

$$\implies I_{peak,y} = \frac{\sin^2 2\theta}{8} (1 - \cos \varepsilon)$$

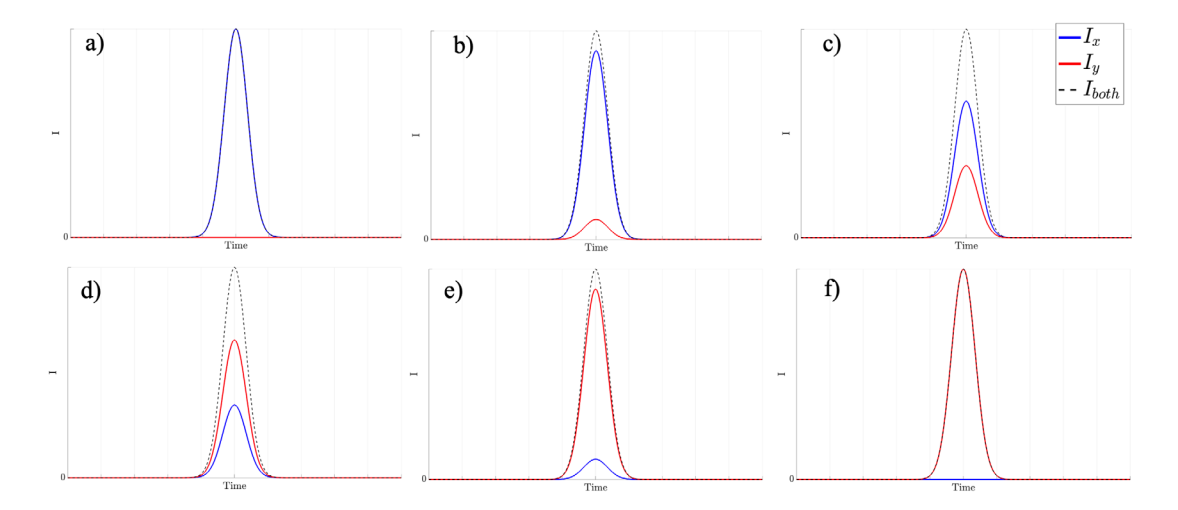


**FIG. 5:** Intensity against time graphs at the detectors and overall. For a,b,c  $I_x$  is the top curve, and for d,e,f  $I_y$  is the top curve.  $\theta = \frac{\pi}{4}$  and alphabetically,  $\varepsilon = 0, \frac{\pi}{5}, \frac{2\pi}{5}, \frac{3\pi}{5}, \frac{4\pi}{5}, \frac{\pi}{5}$ 

where the intensities I are derived from the complex conjugates. Notice that the intensity equations are very similar to that of eq. (1-3). Also, the peak intensities at both detectors are shifted in phase  $\varepsilon$  by a factor of  $\pi$ . The change in the amplitude term involving  $\theta$  as well as modulation in the phase involving  $\varepsilon$  exactly replicates the double slit interference here. Hence, it can be stated that with unique sets of  $(\theta, \varepsilon)$  the interference and hence the WPI can be reconstructed.

### $-\ Which\ Path\ Information\ -$

Comparing the theoretical results to the experimental realisation by Pantaleoni (Fig.6) shows that the total peak intensities  $I_{peak} = I_x + I_y$  agree with the derivations. Starting from the bottom-right diagram of Fig.6 where no WPI is available, shows maximum intensity at the central peak and until the top-left shows WPI with time-distinguishable paths. This can then be summarised as:

$$\theta = k \frac{\pi}{2} \implies \vec{\psi}_{S/L-L/S} \implies \text{WPI Min.} \quad \&$$

$$\theta = (2k-1) \frac{\pi}{4} \implies \vec{\psi}_{S/L-S/L} \implies \text{WPI Max.}$$

where  $k \in \mathbb{Z}$  and S, L stand for Short, Long.

### - DCE Ontology -

We clearly understand that the notion of a delayed-choice is closely tied to the orientation of QWP. Where the WPI is maximised, the double-slit interference pattern is independent of  $\varepsilon$  and on the contrary where WPI is absent, the  $\vec{\psi}$  terms depend on  $\varepsilon$ . Critically, the classical model predicts that until the delayed choice position, light behaves identically in both arms as different components and can be split into different polarisation states.

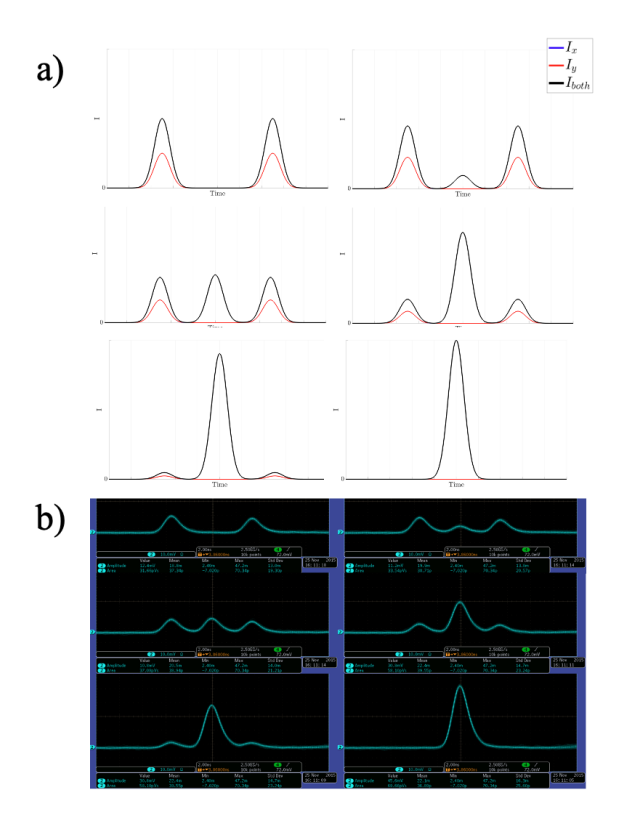


**FIG. 6:** The output intensities versus time for **a**) the analogue's theoretical results with a range of  $\theta = k \frac{\pi}{20}$ ,  $k \in [0, 5]$ . Top line represents the sum intensity,  $I_x$  line output from  $D_x$  which is diminished, and bottom line output from  $D_y$ .  $\varepsilon = 0$  throughout. **b**) The experimental results from Pantaleoni (2017).

This is unlike the quantum theory where the passage of a photon through an arm is determined probabilistically as a superposition of all possible eigenstates. Hence the delayed-choice is classically redundant as the light wave has already made the path 'choice' from the beginning. This implies a lack of retrocausality due to the indistinguishability of the physical situation before interacting with QWP regardless of the WPI status. Without retrocausality, the delayed-choice notion can be interpreted as

follows: "Given that the observation can only occur at the detector in a certain time and space, the 'choice' of measurement is only revealed at the detector once the choice has already been made". The crucial idea that leads to this interpretation is that the notion of the photon's past is not well defined in classical theory and hence, the notion of measurement disturbance is challenged as the information regarding the past is determined **after** the detection. Vice versa, no process can be done in the past to determine the future state of the light.

### - Future Directions -

Adapting analogous models to unveil the classical modelling under the quantum interpretation of various experiments is an attractive area to study in the future. Regarding the Delayed-Choice Double-Slit Experiment, although a great deal of similarities was observed using the proposed analogue, further classical analysis of the delayed choice counterparts (e.g. quantum erasure) is required. The Quantum eraser experiment [3], requires photon entanglement which is famously incompatible with the classical model. The existence of the Wigner quasiprobability distribution [10] also proposes a classical limit that, in this era, limits the derivation of fully compatible models.

### Conclusion

In this paper, we constructed an analogous experiment that adapts the idea of Wheeler's Delayed-Choice experiment to recreate the Double-Slit experiment's results without any reliance on quantum theory. Remodelling Pantaleoni (2017) [7] with adjustments using a VWP to impart phase on the interference, we determined that for a unique set of QWP rotation angles  $\theta$  and VWP phase terms  $\varepsilon$ , the double-slit patterns can be retrieved. The effective presence of QWP results in a minimisation of WPI and maximisation of interfering Gaussians, while the effective lack of QWP results in a maximisation of WPI and minimisation of interfering peaks (time-distinguishable path detections still available). This is shown to be physically analogous to that of the double slit. Regarding the delayed-choice, we conclude that the classical theory is able to mitigate retrocausality by stating that the light's choice prior to the QWP is not well-defined and after the incidence, it is only manifested at the detectors once the choice, and hence the WPI is already determined. Within its causal structure, this analogue offers a simpler explanation for the phenomena at hand, while successfully conforming to experimental results.

### Acknowledgement

We would like to acknowledge the efforts of Giacomo Pantaleoni for providing their thesis on the subject which was the basis for the experimental confirmations, as well as assisting us through discussions. This acknowledgement should also be extended to Sahand Mahmoodian for providing their lecture notes for PHYS2921 (Optics) and assisting us through various discussions. Finally, we would like to acknowledge Angela Karanjai's kind efforts as the supervisor of the project for discussing and assisting with various ideas and most importantly for proposing the research idea.

- Chaves, R., Lemos, G. B., and Pienaar, J. (2018). Causal modeling the delayed-choice experiment. *Physical Review Letters*, 120(19).
- [2] Hecht, E. (2012). Optics. Pearson.
- [3] Kim, Y.-H., Yu, R., Kulik, S. P., Shih, Y., and Scully, M. O. (2000). Delayed "choice" quantum eraser. *Phys. Rev. Lett.*, 84:1–5.
- [4] Marcella, T. V. (2007). Quantum interference with slits. [Note1] Note1. @ plus2@ minus4@ @ plus@ @ plus@ minus2@ Notice that the use of Dirac notation here is purely for contextual reasons and the basis throughout the analysis remains faithful to the classical model.

 $[{\rm Note2}]$   ${\rm Note2}.$  Given experimental values for  $\omega$  and hence  $\tau,$  the overlap for the intensity Gaussians will be minimised.

- [7] Pantaleoni, G. (2016). Quantum mechanical experiments using optical techniques in space. PhD thesis.
- [8] Walborn, S. P., Terra Cunha, M. O., Pádua, S., and Monken, C. H. (2002). Double-slit quantum eraser. Phys. Rev. A, 65:033818.
- [9] Wheeler A., J. (1983). Law without law. Quantum Theory and Measurement, pages 182–213.
- [10] Wigner, E. (1932). On the quantum correction for thermodynamic equilibrium. Phys. Rev., 40:749–759.

### **Optical Element Matrices**

Using the  $\mathcal{B}$  basis for the combined polarisation and propagation direction in Section II, we can define each optical element.

BS

$$\frac{1}{\sqrt{2}} \begin{bmatrix} 1 & i & 0 & 0 \\ i & 1 & 0 & 0 \\ 0 & 0 & 1 & i \\ 0 & 0 & i & 1 \end{bmatrix} \quad \begin{aligned} |H\rangle |X\rangle &\rightarrow \frac{1}{\sqrt{2}} \Big( |H\rangle |X\rangle + i & |H\rangle |Y\rangle \Big), \\ |H\rangle |Y\rangle &\rightarrow \frac{1}{\sqrt{2}} \Big( i & |H\rangle |X\rangle + |H\rangle |Y\rangle \Big), \\ |V\rangle |X\rangle &\rightarrow \frac{1}{\sqrt{2}} \Big( |V\rangle |X\rangle + i & |V\rangle |Y\rangle \Big), \\ |V\rangle |Y\rangle &\rightarrow \frac{1}{\sqrt{2}} \Big( i & |V\rangle |X\rangle + |V\rangle |Y\rangle \Big). \end{aligned}$$

Mirrors

$$\begin{bmatrix} 0 & 1 & 0 & 0 \\ 1 & 0 & 0 & 0 \\ 0 & 0 & 0 & 1 \\ 0 & 0 & 1 & 0 \end{bmatrix} \quad \begin{array}{l} |H\rangle \, |X\rangle \rightarrow |H\rangle \, |Y\rangle \,, \\ |H\rangle \, |Y\rangle \rightarrow |H\rangle \, |X\rangle \,, \\ |V\rangle \, |X\rangle \rightarrow |V\rangle \, |Y\rangle \,, \\ |V\rangle \, |Y\rangle \rightarrow |V\rangle \, |Y\rangle \,. \end{array}$$

$$\begin{bmatrix} 1 & 0 & 0 & 0 \\ 0 & 1 & 0 & 0 \\ 0 & 0 & 0 & i \\ 0 & 0 & i & 0 \end{bmatrix} \quad \begin{array}{l} |H\rangle \, |X\rangle \rightarrow |H\rangle \, |X\rangle \,, \\ |H\rangle \, |Y\rangle \rightarrow |H\rangle \, |Y\rangle \,, \\ |V\rangle \, |X\rangle \rightarrow i \, |V\rangle \, |Y\rangle \,, \\ |V\rangle \, |Y\rangle \rightarrow i \, |V\rangle \, |X\rangle \,. \end{array}$$

QWP (First Pass)

QWP is placed at an angle  $\theta$  from the horizontal polarisation axis on the first passage.

$$\begin{bmatrix} 1 & 0 & 0 & 0 \\ 0 & \cos^2\theta + i\sin^2\theta & 0 & (1-i)\cos\theta\sin\theta \\ 0 & 0 & 1 & 0 \\ 0 & (1-i)\cos\theta\sin\theta & 0 & i\cos^2\theta + \sin^2\theta \end{bmatrix}$$

$$\begin{split} |H\rangle |X\rangle &\to |H\rangle |X\rangle \,, \\ |H\rangle |Y\rangle &\to \left( (\cos^2\theta + i\sin^2\theta) \,|H\rangle \right. \\ &\quad + (1-i)\cos\theta\,\sin\theta\, |V\rangle \right) |Y\rangle \,, \\ |V\rangle |X\rangle &\to |V\rangle |X\rangle \,, \\ |V\rangle |Y\rangle &\to \left( (1-i)\cos\theta\,\sin\theta\, |H\rangle \right. \\ &\quad + (i\cos^2\theta + \sin^2\theta) |V\rangle \right) |Y\rangle \,. \end{split}$$

SBM

$$\begin{bmatrix} 1 & 0 & 0 & 0 \\ 0 & 1 & 0 & 0 \\ 0 & 0 & 1 & 0 \\ 0 & 0 & 0 & -1 \end{bmatrix}$$

QWP (Second Pass)

QWP is placed at an angle  $\pi - \theta$  from the horizontal polarisation axis on the first passage.

$$\begin{bmatrix} 1 & 0 & 0 & 0 \\ 0 & \cos^2\theta + i\sin^2\theta & 0 & (i-1)\cos\theta\sin\theta \\ 0 & 0 & 1 & 0 \\ 0 & (i-1)\cos\theta\sin\theta & 0 & i\cos^2\theta + \sin^2\theta \end{bmatrix}$$

$$\begin{split} |H\rangle \, |X\rangle &\to |H\rangle \, |X\rangle \,, \\ |H\rangle \, |Y\rangle &\to \left( (\cos^2\theta + i\sin^2\theta) \, |H\rangle \right. \\ &\quad + (i-1)\cos\theta \, \sin\theta \, |V\rangle \right) |Y\rangle \,, \\ |V\rangle \, |X\rangle &\to |V\rangle \, |X\rangle \,, \\ |V\rangle \, |Y\rangle &\to \left( (i-1)\cos\theta \, \sin\theta \, |H\rangle \right. \\ &\quad + \left( i\cos^2\theta + \sin^2\theta \right) |V\rangle \right) |Y\rangle \,. \end{split}$$

HWP

$$\frac{1}{\sqrt{2}} \begin{bmatrix} 1 & 0 & 1 & 0 \\ 0 & \sqrt{2} & 0 & 0 \\ 1 & 0 & -1 & 0 \\ 0 & 0 & 0 & \sqrt{2} \end{bmatrix}$$
$$|H\rangle |X\rangle \rightarrow \frac{1}{\sqrt{2}} (|H\rangle |X\rangle + |V\rangle |X\rangle),$$
$$|H\rangle |Y\rangle \rightarrow |H\rangle |Y\rangle,$$
$$|V\rangle |X\rangle \rightarrow \frac{1}{\sqrt{2}} (|H\rangle |X\rangle - |V\rangle |X\rangle),$$
$$|V\rangle |Y\rangle \rightarrow |V\rangle |Y\rangle.$$

VWP

$$\begin{bmatrix} 1 & 0 & 0 & 0 \\ 0 & 1 & 0 & 0 \\ 0 & 0 & e^{i\varepsilon} & 0 \\ 0 & 0 & 0 & 1 \end{bmatrix} \quad \begin{array}{l} |H\rangle \, |X\rangle \rightarrow |H\rangle \, |X\rangle \,, \\ |H\rangle \, |Y\rangle \rightarrow |H\rangle \, |Y\rangle \,, \\ |V\rangle \, |X\rangle \rightarrow e^{i\varepsilon} \, |V\rangle \, |X\rangle \,, \\ |V\rangle \, |Y\rangle \rightarrow |V\rangle \, |Y\rangle \,. \end{array}$$

And that is a wrap for another issue of The Physics Society's homegrown magazine, Jeremy! We hope you took something away from the fascinating world of measure theory, or the fuzziness in our perception of wave-particle duality. Maybe after reading this issue, you have become encouraged to do some more 'napking calculations' when a moment of inspiration strikes, or maybe you have become more interested in the study of proteins on mice. Either way, we are glad you came along this journey!

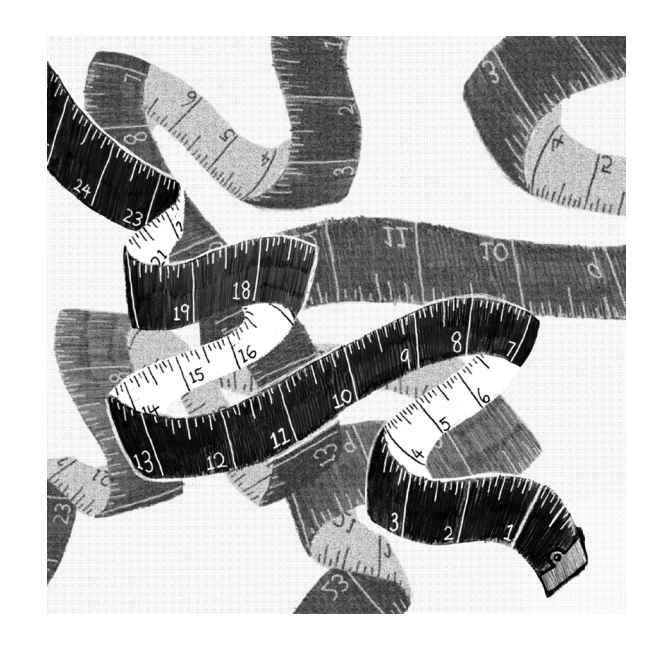
And don't forget to follow our socials on Instagram and the PhySoc website.

Also do not hesitate to contact us via **jeremy.physoc@gmail.com** for ideas, article submissions, or anything else.

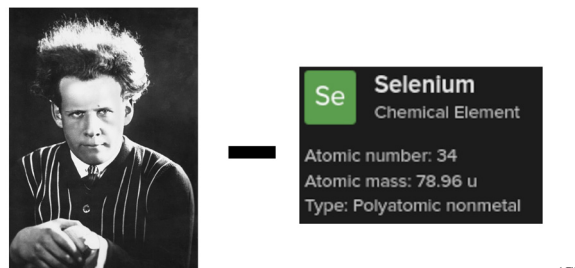








### Guess the rebus!





Make sure to follow the Puzzle Society, who kindly gave us puzzles for this sec-

(Clue: Famous Physicist)

# **Geocaching Puzzle**

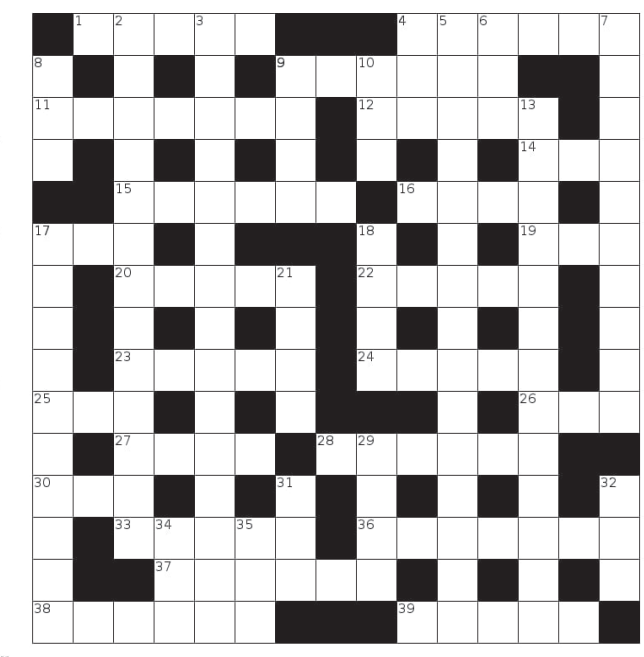
The Sydney University Graffiti tunnel operates on the position states |Science Road | and |Manning Road | (i.e. users can travel between Science Road and Manning Road, bypassing the Quadrangle). Anyone is free to visit and create artwork in the tunnel!

Clue: A flashlight might help.

### **Crossword of the Issue**

### **ACROSS**

- 1. What Fred loves
- 4. A workholding tool
- 9. Where we all went
- 11. A large jar for wine in ancient greece
- **12.** Like running fingers through your hair
- 14. A ratio much like 29D
- **15.** A way to cook a steak?
- 16. Norse god that shapeshifted into a mare and gave birth to a horse with 8 legs
- 17. Opposite of Id
- 19. Something that a journalist might recieve
- 20. Boxes
- 22. What I feel like in my math classes sometimes
- 23. Type of poem, including the Illiad
- 24. \_\_\_\_\_ 's theorem, or the \_\_\_\_ Tao theorem.
- 25. Drink traditionaly found on navy ship
- **26.** You can feel dread here
- 27. Study for the \_\_\_\_ (Kinda bad that we do)
- 28. A type of rodent found in South America
- 30. Smallest of a set
- 33. Gang of three
- 36. Fisher or law perhaps
- **37.** Gave shelter to
- 38. Claws
- 39. The air version of this is the greatest usage of thermodynamics, no I will not be taking questions



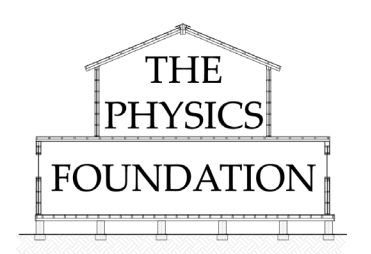
### DOWN

- In diplomacy, when two countries start talking to each other again.
- 3. What I'm doing when really should be working but instead im just sitting around and not working and now I have to do more work because Ive been sitting around not working
- **4.** What people do to babies, and pigeons do to people
- 5. {|N}/{|P}
- 6. Law degree postnominal
- 7. Reusing and reqriting over paper
- 8. The practical part of the course

- 9. You better call him
- **10.** The hormone detected in pregnancy tests
- 13. An absolute likeness
- 3. What I'm doing when I 17. I was terrible at doing really should be these, done in 8D
  - 18. The shape of the LHC
  - 21. If a fish swapped the B for an S and snapped its fingers at you
  - 29. AU metal
  - 31. Run on youtube videos
  - 32. You go to be healthy
  - 34. Resistivity symbol
  - **35.** Where we are, contracted

We would like to thank our generous sponsors:











Follow our socials

@jeremy\_usyd

for the solution to the puzzles!

# Our Supporters

*Jeremy* is a student-run, non-profit group that strives to bring scientifically accurate and enjoyable articles to a wide array of audiences. We are thankful of our sponsors for making this task possible.

If you are also interested in donating to or sponsoring *Jeremy*, please reach out to out team!

